Dynamic Localized Failure of Soils via Nonlocal Poromechanics Model: A Case Study of the Lower San Fernando Dam Failure

Shashank Menon¹ and Xiaoyu Song Ph.D.²

¹Engineering School of Sustainable Infrastructure and Environment, Univ. of Florida, Gainesville, FL

²Associate Professor, Engineering School of Sustainable Infrastructure and Environment, Univ. of Florida, Gainesville, FL (corresponding author). Email: xysong@ufl.edu

ABSTRACT

In this article, a recently developed nonlocal poromechanics model for geomaterials is applied to analyze the dynamic response of the Lower San Fernando Dam during the 1971 San Fernando earthquake. During the earthquake, the dam experienced a major flow failure in the upstream slope. Field investigations in the immediate aftermath indicated that the horizontal movement in the upper slope of the San Fernando Dam was caused by the liquefaction and weakening of the hydraulic fill materials in certain zones in the dam. Large blocks of mostly intact soil from the upstream section of the dam moved into the reservoir, riding over on the liquefied soil. Field analysis suggested that a significant pressure buildup occurred in the central region of the dam due to cyclic loading that later migrated to the upstream "toe" where it triggered failure and subsequently a sliding flow. To demonstrate that the proposed nonlocal poromechanics is realistic and relevant to the solution of large-scale, nonlinear, and coupled analysis, we conduct a two-stage seismic analysis of the Lower San Fernando Dam. First, an elastic analysis under quasi-static condition was carried out to determine initial effective stress and water pressure distributions. Second, a fully nonlinear dynamic analysis was performed with the earthquake load modeled as a base excitation following recorded acceleration profiles. The results have demonstrated that the proposed nonlocal poromechanics model is robust in modeling the localized failure of geomaterials under seismic loading by capturing the location and mode of failure observed in the field.

INTRODUCTION

The dynamic behavior of geomaterials is strongly influenced by the coupled interactions between the solid skeleton and pore fluid, as seen in the process of liquefaction and strain localization. A soil deposit subject to cyclic shear loading, most observed during earthquakes, develops excess pore pressures that dissipate towards the surface causing uneven settlement, foundation collapse, and extensive structural damage as seen in Niigata, 1964 (7.6 M_w) (Seed & Idriss 1967). The development of excess pore pressure in soils can cause a drop in structural strength associated with loss of matric suction leading to rapid and catastrophic localization of plastic strains in a narrow zone, in a process that is termed strain localization (Malvick et al. 2008). Strain localization of geomaterials under the quasi-static condition has been the subject of intense research activity under variably saturated conditions but dynamic strain localization remains a fledgling field of study. Numerical analysis of strain localization in geomaterials presents certain technical challenges. It is well-known that modeling strain-softening using classical continuum formulations, without an internal length scale, leads to spurious mesh

sensitivity of the localized zone and vanishing plastic dissipation. Non-local continuum theories have emerged as powerful tools to regularize the boundary value problem in the strain-softening regime by restricting the width of the localized zone using an explicitly defined characteristic length scale parameter. Experimental testing has revealed that the thickness of shear bands in geomaterials can vary between the order of the size of several grains or meters in the field scale (e.g., Mühlhaus and Vardoulakis 1987). In this study, we apply a recently developed non-local unsaturated poromechanics framework (Menon & Song 2020) to run a case study of the liquefaction in the Lower San Fernando Dam. The effective force vector state and fluid flow scalar state (Silling et al. 2007, Song & Silling 2020) are used to cast the force balance equation and mass balance equation for modeling the coupled mechanical and hydraulic behavior of soils. The multiphase constitutive correspondence principle (Song & Silling 2020) is used to determine the peridynamic force and fluid flow states from classical elastoplastic models (e.g., Song and Khalili 2019) and the generalized Darcy's law. The case study of the failure of the Lower San Fernando dam (see Seed et al. 1975 a & b) showcases the robustness of this nonlocal poromechanics framework for modeling dynamic localized failure of geomaterials on the field scale under earthquake loads.

MATHEMATICAL FORMULATION

The proposed nonlocal poromechanics framework is briefly summarized in this section. A point on the notation used in this study: boldface represents a vector quantity; bold italics represent a tensor quantity and underscores are used to differentiate peridynamic state quantities from classical point associated quantities. In this model, it is assumed that geomaterials can be conceptualized as a body consisting of finite material points interacting with each other over a finite distance called the horizon. The horizon is an explicitly defined length scale parameter that demarcates the neighborhood, H_x , of a material point x. All material field variables are tracked by mathematical quantities termed 'states'. Each material point has two types of degree of freedom, i.e., displacement and fluid pressure. As such, the formulation in the article is a u-p formulation as in the classical computational poromechanics (see, Zienkiewicz et al., 1999). Deformation and fluid flow are imposed along a 'bond' between two material points x and x',

$$\underline{\mathbf{X}} = \mathbf{\xi} = \mathbf{x}' - \mathbf{x},$$

where $\underline{\mathbf{X}} = \boldsymbol{\xi}$ is the bond between a point and its neighbor and is the relative position vector from \mathbf{x} to \mathbf{x}' . For the skeleton, the primary variable is the deformation vector state $\underline{\mathbf{Y}}(\boldsymbol{\xi})$ associated with individual interactions between material points,

$$\underline{Y}\langle \xi \rangle = y'(x') - y(x) \quad \text{,} \quad y(x) = x + u \quad \text{,} \quad y'(x') = x' + u',$$

where **u** and **u**' are the displacements at material points **x** and **x**' and the $\langle \cdot \rangle$ is the bond with which the deformation state is associated. The derived variable is the effective force vector state $\underline{\tilde{T}}\langle \xi \rangle$ which is obtained from the skeleton resistance to deformation and can be decomposed as,

$$\underline{\widetilde{\mathbf{T}}}[\mathbf{x}]\langle \boldsymbol{\xi} \rangle = \underline{\mathbf{T}}[\mathbf{x}]\langle \boldsymbol{\xi} \rangle + \underline{\mathbf{T}}_{\mathcal{W}}[\mathbf{x}]\langle \boldsymbol{\xi} \rangle,$$

where $\underline{\mathbf{T}}$ is the total force state and $\underline{\mathbf{T}}_{w}$ is the pressure force state related to the pore fluid pressure. In this article the sign convention in continuum mechanics is followed, e.g., deformation in tension is positive and compressive pore pressure is positive. The momentum balance is expressed as,

$$\begin{split} \int_{H_x} & \left(\underline{\widetilde{\mathbf{T}}}[\mathbf{x}] \langle \boldsymbol{\xi} \rangle - \underline{\mathbf{T}}_w[\mathbf{x}] \langle \boldsymbol{\xi} \rangle \right) - \left(\underline{\widetilde{\mathbf{T}}}'[\mathbf{x}'] \langle -\boldsymbol{\xi} \rangle - \underline{\mathbf{T}}'_w[\mathbf{x}'] \langle -\boldsymbol{\xi} \rangle \right) dV' + \rho_s (1 - \varphi) \cdot \mathbf{g} + \varphi \rho_w \cdot \mathbf{g} \\ &= (\rho_s (1 - \varphi) + \varphi \rho_w) \mathbf{a}, \end{split}$$

where ρ_s is the density of soil, ϕ is the porosity of soil, g is the gravity acceleration vector, ρ_w is the density of water, a is the acceleration vector associated with deformation, and the integral term implies a spatial summation over all material points in the horizon of x. The effective force state and pressure force state in a bond are related to the effective stress tensor $\overline{\sigma}$ and pore pressure p_w as follows,

$$\underline{\widetilde{\mathbf{T}}}\langle \boldsymbol{\xi} \rangle = \omega \langle \boldsymbol{\xi} \rangle J \overline{\boldsymbol{\sigma}} \overline{\boldsymbol{F}}^{-T} \boldsymbol{K}^{-1} \boldsymbol{\xi}, \underline{\mathbf{T}}_{\!\scriptscriptstyle W} \langle \boldsymbol{\xi} \rangle = \omega \langle \boldsymbol{\xi} \rangle J p_{\scriptscriptstyle W} \overline{\boldsymbol{F}}^{-T} \boldsymbol{K}^{-1} \boldsymbol{\xi}$$

where \overline{F} is the nonlocal deformation gradient that is assembled over all deformation vector states in the horizon through the notion of a nonlocal spatial gradient,

$$\overline{F} = \left[\int_{H_X} \omega \underline{\mathbf{Y}} \langle \boldsymbol{\xi} \rangle \otimes \underline{\mathbf{X}} \langle \boldsymbol{\xi} \rangle \, \mathrm{dV'} \right] \mathbf{K}^{-1} \quad , \quad \boldsymbol{K} = \int_{H_X} \omega \,\underline{\mathbf{X}} \, \langle \boldsymbol{\xi} \rangle \otimes \underline{\mathbf{X}} \, \langle \boldsymbol{\xi} \rangle \, \mathrm{dV'},$$

where K is the shape tensor, J is the determinant of the deformation gradient, \otimes stands for a tensor product between two vectors and ω is a weighting function (Silling et al 2007). The effective stress tensor is determined using a previously developed nonlocal elastoplastic model (see Song & Menon 2018) of the Cam-Clay type. In this model, the effective stress is determined by an isotropic elastic stress-strain relationship. The yielding function is

$$f(\overline{\boldsymbol{\sigma}}, p_c) = \frac{q^2}{M^2} + p'(p' - p_c),$$

where q is the deviator stress, p' is the mean effective stress, M is the slope of critical state line, and p_c is the pre-consolidation pressure which serves as a hardening parameter as follows,

$$\dot{\mathbf{p}}_{c} = \frac{-\mathbf{p}_{c}}{\tilde{\lambda} - \tilde{\kappa}} \mathrm{tr}(\dot{\boldsymbol{\varepsilon}}^{p}),$$

where $\tilde{\lambda}$ is the compression index and $\tilde{\kappa}$ is the swelling index, and $\dot{\epsilon}^p$ is the rate plastic strain. The associative flow rule is assumed as

$$\dot{\boldsymbol{\varepsilon}}^{\mathrm{p}} = \dot{\lambda} \frac{\partial f}{\partial \overline{\boldsymbol{\sigma}}}$$

where $\dot{\lambda}$ is the non-negative plastic multiplier. The objective of this study is to model failure inception in a field-scale problem and conduct a preliminary validation of the formulation for

analysis of real engineering problems. We note that to better model the response of soil under cyclic loading a more sophisticated constitutive model (e.g., bounding surface model) will be needed, which is beyond the scope of this present article. For the fluid transport, the fundamental variable is the pressure potential state $\Phi_w(\xi)$ which takes the form,

$$\underline{\Phi}_{w} = \mathbf{p}_{w}'(\mathbf{x}') - \mathbf{p}_{w}(\mathbf{x}),$$

where p_w is the pore water pressure. Then, the classical flux vector \mathbf{q}_w at any mixed material point can be determined by applying Darcy's law as described below,

$$\mathbf{q}_{\mathrm{w}} = -k_{w} \big(\widetilde{\mathbf{\nabla}} \Phi_{w} - \rho_{w} \mathbf{a} \big) \quad , \quad \widetilde{\mathbf{\nabla}} \Phi_{\mathrm{w}} = \int_{H_{x}} \omega \langle \mathbf{\xi} \rangle \, \underline{\mathbf{q}}_{w} \langle \mathbf{\xi} \rangle \, \underline{\mathbf{X}} \langle \mathbf{\xi} \rangle dV',$$

where, $\nabla \Phi_w$ is the nonlocal fluid pressure gradient determined by integrating all pressure potential states over the horizon and k_w is the hydraulic conductivity of pore water. The peridynamic fluid flow state, \underline{Q}_w is the volumetric rate of flow through a bond and is related to classical flux through Darcy's law as follows,

$$Q_w = \omega(\mathbf{q}_w - k_w \rho_w a) \mathbf{K}^{-1} \boldsymbol{\xi}.$$

The coupling term in the mass balance, the divergence of velocity in classical poromechanics, can be determined as follows,

$$\dot{V} = \left[\int_{H_X} \omega(\dot{\mathbf{u}}' - \dot{\mathbf{u}}) \, \underline{\mathbf{X}} \langle \mathbf{\xi} \rangle \, \mathrm{dV}' \right] \mathbf{K}^{-1}$$

using a nonlocal divergence operator. The mass balance equation for saturated geomaterials is written as

$$\frac{\Phi}{K_{w}} \frac{d}{dt} (p_{w}) + \left[\int_{H_{x}} \omega(\dot{\mathbf{u}}' - \dot{\mathbf{u}}) \, \underline{\mathbf{X}} \langle \boldsymbol{\xi} \rangle \, dV' \right] \mathbf{K}^{-1} + \frac{1}{\rho_{w}} \int_{H_{x}} \left(\underline{Q}_{w}[\mathbf{x}] \langle \boldsymbol{\xi} \rangle - \underline{Q}'_{w}[\mathbf{x}'] \langle -\boldsymbol{\xi} \rangle \right) dV'$$

$$= 0$$

where K_w is the bulk modulus of water, and \underline{Q}_w and \underline{Q}'_w are the fluid flow states at \mathbf{x} and \mathbf{x}' . The mathematical model has been implemented numerically through an explicit two-phase meshfree method. We note that the inclusion of the length scale in the governing equations of the coupled system serve to regularize the localization problem and maintain mesh insensitivity in the post-strain localization regime.

PROBLEM DESCRIPTION

On the 9th of February 1971 thrust faulting on the Sierra Madre fault-line triggered the San-Fernando earthquake (Richter Magnitude 6.6) (Sykora 2019). This earthquake caused an estimated \$550 million in damage, largely to buildings and a major hospital, killed 50 people, and left hundreds trapped in the rubble. The duration of strong ground shaking was approximately 15 seconds. High-frequency peak accelerations of 1.25 g were recorded in two

horizontal directions, at AR-240 at Pacoima Dam, located near the very center of the seismic event, these being the highest ground accelerations recorded for earthquakes at that point (Trifunac & Hudson 1971). As a result, the Lower San Fernando Dam developed a major slide in the upstream slope and crest. The field investigation (Seed et al. 1975b) showed that the slide occurred due to the liquefaction of a zone of hydraulic sand fill in the upstream slope. The hydraulic fill consisted of fine to coarse sands, silty sands and layered sands, silts, and clays. The zone that liquefied and developed flow-type deformations was roughly triangular, and investigations conducted in the aftermath suggested that practically all the soil within this zone participated in the flow-type deformations.

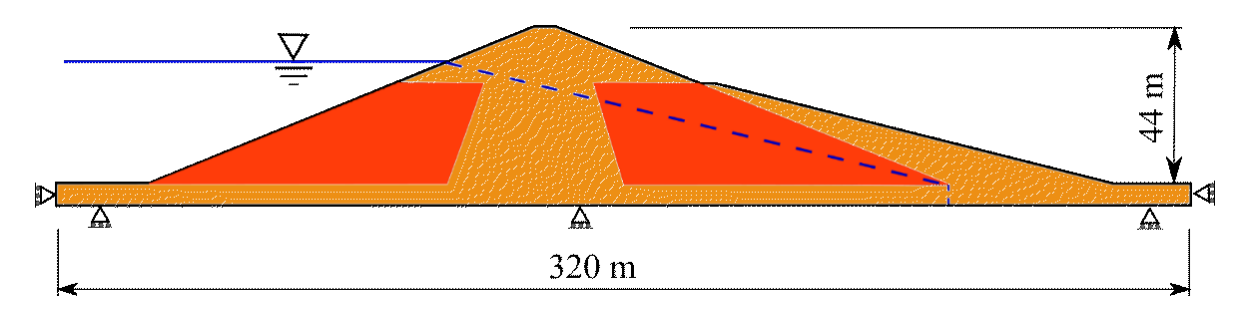


Figure 1 Schematic of the Lower San Fernando Dam for the numerical simulation in which the clay core is outlined in black and the hydraulic fill is in red.

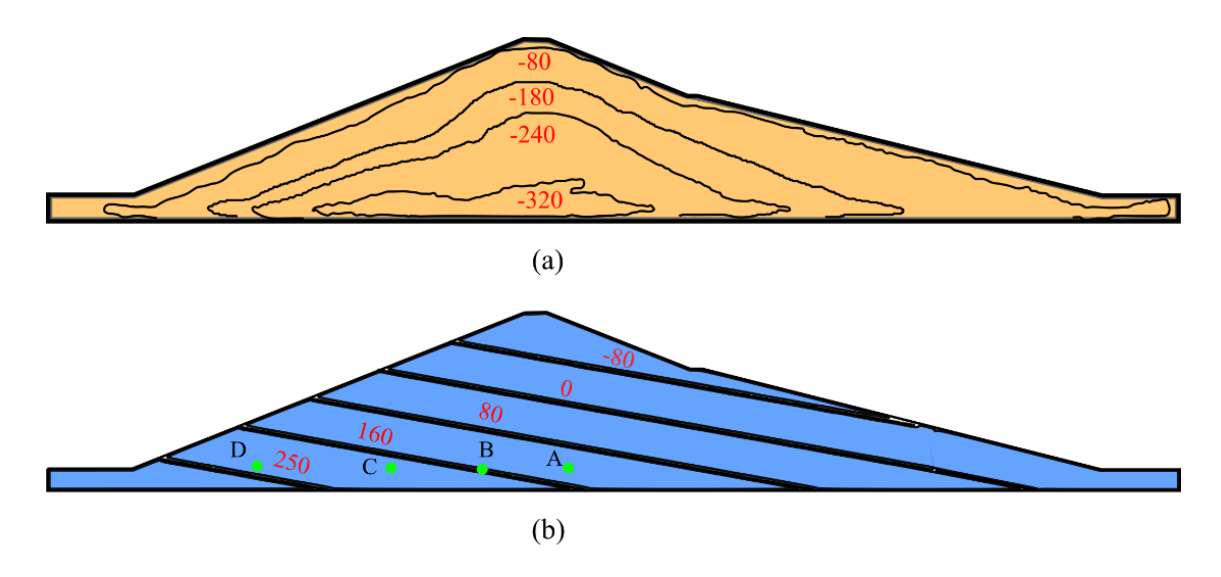


Figure 2 The initial distribution (in kPa) of the (a) vertical effective stress and (b) fluid pressure in the dam.

Figure 1 shows an idealization of the San Fernando dam utilized in this study and boundary conditions applied to the domain. The base of the domain is constrained against vertical motion while the horizontal ends are both constrained against lateral deformation. Outside the dam, the solid blue line marks the level of water on the upstream slope in the reservoir, while inside the dam the dashed blue line separates the saturated zone from the unsaturated zone. The problem domain is discretized into 24,000 mixed material points with a center-to-center distance 0.6 m. A

length scale (i.e., horizon) of 1.3 m is chosen. The rollers in Figure 1 represent sliding boundary conditions: the base is constrained to lateral motion only while the two extreme ends of the dam can only move vertically. The bulk of the dam is made of fines of various types (Seed et al. 1975a) which we have simplified in our analysis to a single slightly overconsolidated clay (shaded in brown in Figure 1). The remainder of the dam is composed of looser and weaker hydraulic filler material (shaded in red in Figure 1).

The elastic skeleton material properties are chosen following (Zienkiewicz et al. 1999): Young's modulus $K = 30 \times 10^3$ kPa and Poisson's ratio $\nu = 0.2857$. For the remaining input parameters, $\tilde{\kappa} = 0.01$, $\tilde{\lambda} = 0.16$, the over-consolidation ratio is 1.5, the slope of critical state line is 1.0, and the stabilization parameter G = 0.1. The fluid stiffness is 2.2×10^6 kPa. The clayey core has a hydraulic conductivity of 10^{-3} m/s, while the hydraulic filler has a larger conductivity of 10^{-2} m/s

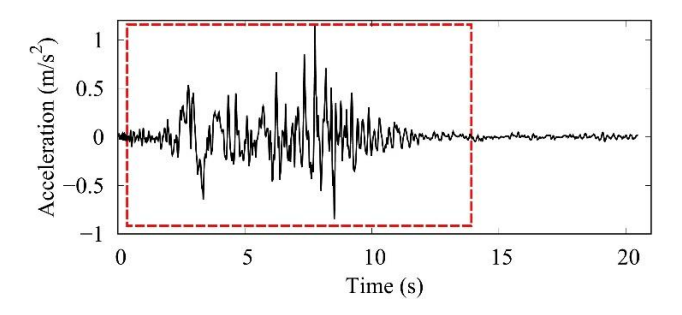


Figure 3 The acceleration profile of the San Fernando Valley Earthquake taken from the Pacoima Dam accelerogram located 7 miles NE of the Lower San Fernando Valley Dam (available at https://strongmotioncenter.org/)

An elastic quasi-static step is used to generate geostatic stress and initial pressure distribution, shown in Figure 2 (a) and (b) respectively. With the crest of the dam taken as the datum, effective skeleton stress is calculated using the gravitational load acting on the soil in the dam. Pore pressure directly beneath the reservoir is assigned using the relationship, $p_0 = \rho_w gh$, with h denoting the height of the water above the point. Pore pressure distribution in the bulk of the domain, away from the reservoir, is assigned based on the distance from the phreatic line with pore pressure developing beneath the phreatic line (the blue dashed line in Figure 1) and matric suction developing above it. In the second stage, a fully coupled plastic dynamic analysis of the earthquake motion is performed. The earthquake acceleration profile used in this analysis is depicted in Figure 3. Note that the strong ground motion only lasts for 12 seconds. This acceleration profile is applied to the base of the dam. The region outlined in red marks the portion of the profile used.

RESULTS

Figure 4 draws the contours of the (a) plastic shear and (b) displacement vectors in the domain in the aftermath of the shaking. From the field data analysis, the maximum deformation occurred at the toe of the dam on the upstream slope. The contours of displacement in Figure 4(b), show the probable failure mode: a slide at the upstream slope. The numerical results show that the maximum plastic deformation has concentrated in a banded zone extending from beneath the reservoir into the core of the dam. It is noted that the

maximum magnitude of plastic strain occurred in the region with the looser hydraulic fill which corresponds to the zone of liquefaction noted by (Seed et al 1975a). While there is noticeable settlement at the crest of the dam, the downstream slope remains largely unchanged from the initial configuration. This also matches the observations made by the field analysis. Given the lack of any suction-hardening model in the constitutive relationship, it appears that the cohesion developed in the unsaturated zone alone is physically significant. Indeed, in an analysis conducted by Zienkiewicz et al. (1999) the authors found that ignoring the suction cohesion triggers an almost instant collapse in the downstream slope, contradicting the actual failure observed in the dam.

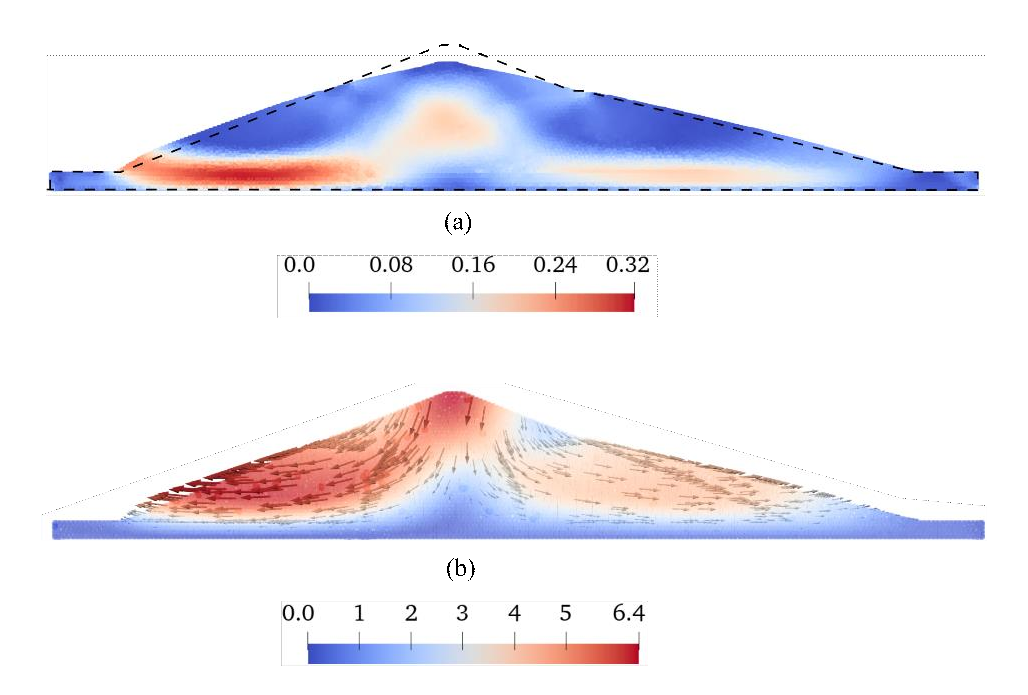


Figure 4 Contours of the deformed configuration of the dam depicting (a) plastic shear strain and (b) direction vectors of the displacement.

Figure 5 plots the evolution of vertical displacements at selected points A, B, C and D depicted in Figure 2(b).

There is a noticeable increase in vertical displacement (settlement) in the aftermath of the shaking. The continuing settlement is caused by plastic deformation that occurs after the shaking has ceased. This is likely caused by the generation of excess pore pressure. Figure 6 plots the evolution of excess pore pressure (in hundreds of KPa) at the selected points in the dam structure. The magnitude of excess pressure developed in the duration of shaking are largest at the center of the dam (tracked at points A and B). Points C and D, which are nearer to the upstream toe of the dam develop lower values of excess pressure during the shaking. However, the pressure developed in the central bulk of the dam appears to dissipate rapidly once shaking ceases at approximately 12 s. The excess pressure at the toe remains relatively consistent towards the end of the simulation. These trends in the data lend credence to the failure mechanism proposed by Seed et al. 1975a: excess pressure developed largely in the core and migrated towards the toe triggering failure in the looser filler material.

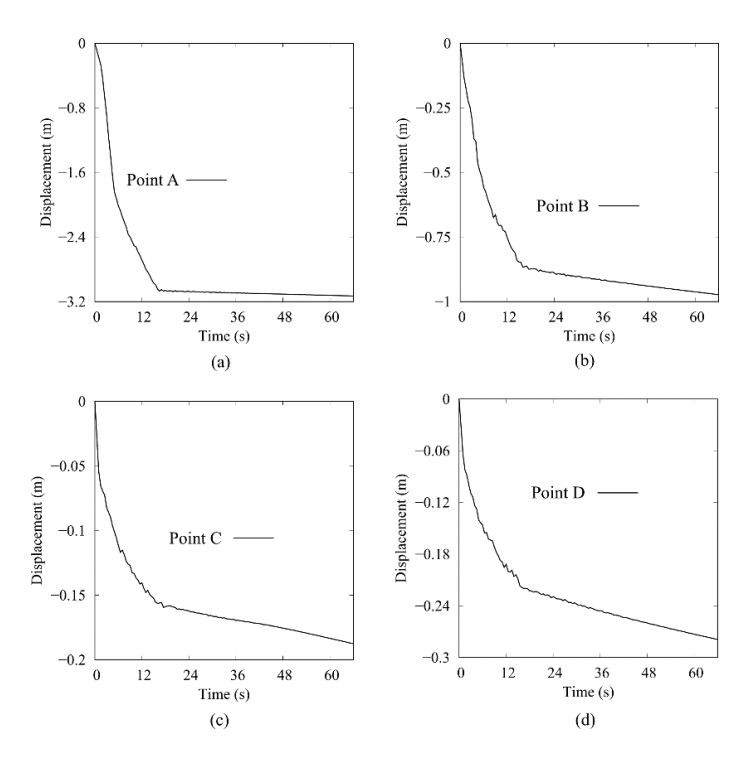


Figure 5 Plots of the evolution of vertical displacement over time at select points in the dam shown in Figure 4.

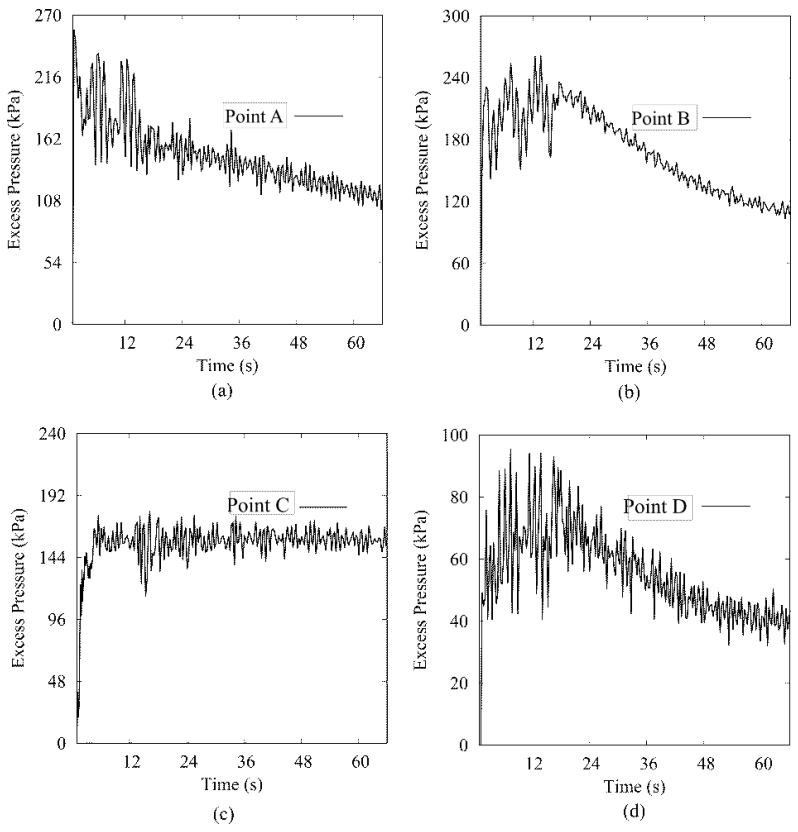


Figure 6 Plots of the evolution of pressure at selected points in the dam (shown in Figure 2(b)).

As a final step, the uniqueness of the solution is validated by rerunning the simulation with a finer discretization of 51,000 mixed material points while all other simulation parameters remain the same. Figure 7 plots the contours of equivalent plastic shear strain in the domain for both discretizations t = 12 s. It is apparent that for both discretizations used, the width of the localized zone, as well as the intensity of plastic deformation, are in good agreement. Furthermore, as shown in Figure 8 the plot comparing the evolution of equivalent plastic shear strain at identical locations in the two discretizations are well-matched.

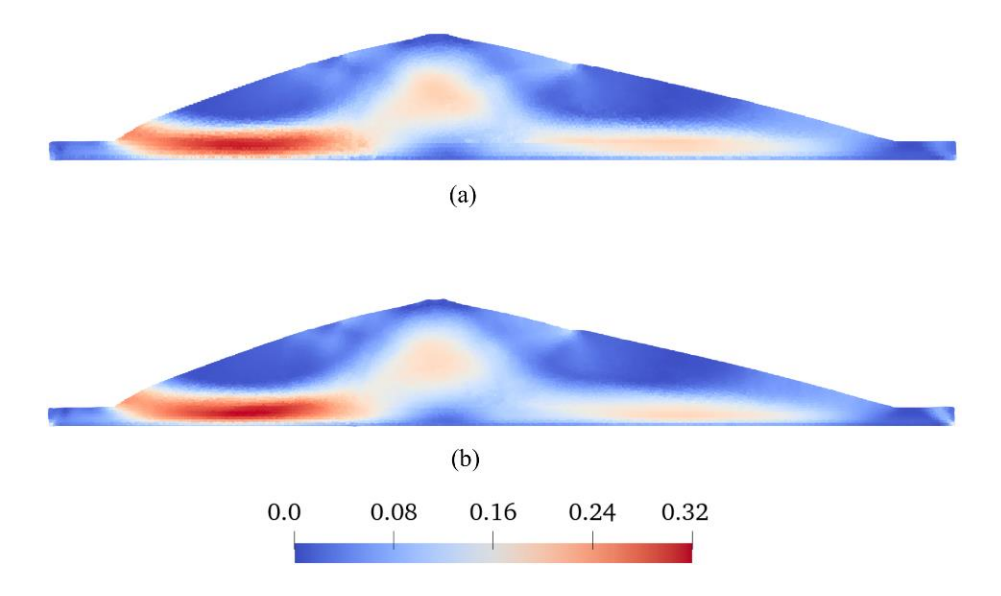


Figure 7 Contours of equivalent plastic shear strain in a discretization with (a) 24,000 mixed material points and (b) 51,000 mixed material points.

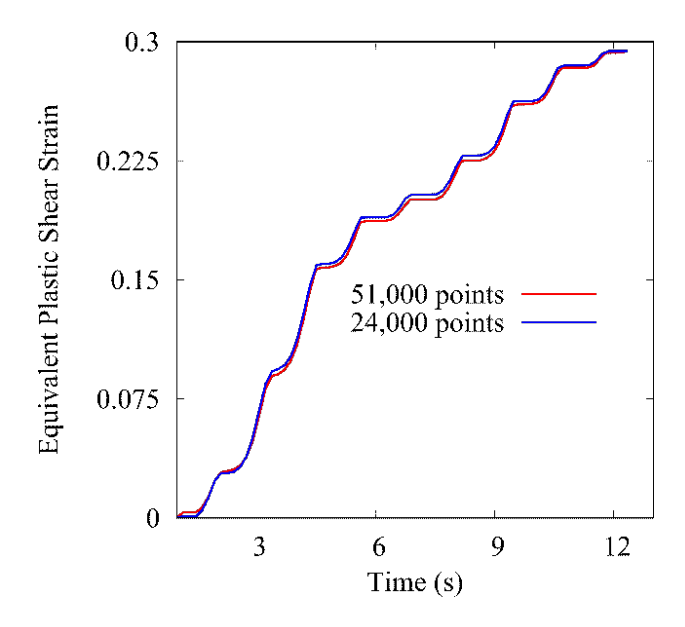


Figure 8 Equivalent plastic shear strain at the same point by simulations with two discretization schemes.

CONCLUSION

A nonlocal dynamic poromechanics model was applied to simulate the failure of the Lower San Fernando Dam during the 1971 earthquake. The numerical results demonstrated that the proposed numerical method can predict the mode and location of the failure that occurred in the dam. The base excitation caused plastic deformation which in turn generated excess pore water pressures. The increased water pressure may further weaken the soil in the upstream slope of the dam that eventually caused the dam failure. On the other hand, the downstream slope remained relatively unchanged from its initial configuration due to the denser clay berm and its location above the phreatic line, e.g., the large suction developed downstream may contribute to its stability. It is found that proposed nonlocal numerical method is insensitive to the spatial discretization as typically found in the numerial method based on classical poromecahnics. It can be concluded that the proposed nonlocal poromechanics model is robust in modeling dynamic localized failure at the field scale.

REFERENCES

- Malvick, E. J., Kutter, B. L., and Boulanger, R. W. (2008). Post-shaking shear strain localization in a centrifuge model of a saturated sand slope. *Journal of Geotechnical and Geoenvironmental Engineering*, 134(2), 164-174.
- Menon, S., and Song, X. (2020). A computational periporomechanics model for localized failure in unsaturated porous media. https://arxiv.org/abs/2010.15793.
- Mokni, M., and Desrues, J. (1999). Strain localization measurements in undrained plane-strain biaxial tests on Hostun RF sand. *Mechanics of Cohesive-frictional Materials*, 4(4), 419-441.
- Mühlhaus, H. B., and Vardoulakis, I. (1987). The thickness of shear bands in granular materials. *Geotechnique*, 37(3), 271-283.
- Seed, H. B., and Idriss, I. M. (1967). Analysis of soil liquefaction: Niigata earthquake. *Journal of the Soil Mechanics and Foundations Division*, 93(3), 83-108.
- Seed, H. B., Lee, K. L., and Idriss, I. M., et al. (1975a). The slides in the San Fernando dams during the earthquake of February 9, 1971. *Journal of Geotechnical and Geoenvironmental Engineering*, 101(ASCE# 11449 Proceeding).
- Seed, H. B., Idriss, I. M., and Lee, K. L., et al. (1975b). Dynamic analysis of the slide in the Lower San Fernando Dam during the earthquake of February 9, 1971. *Journal of Geotechnical and Geoenvironmental Engineering*, 101(ASCE# 11541 Proceeding).
- Silling, S. A., Epton, M., and Weckner, O., et al. (2007). Peridynamic states and constitutive modeling. *Journal of Elasticity*, 88(2), 151-184.
- Song, X., Wang, K., and Ye, M. (2018). Localized failure in unsaturated soils under non-isothermal conditions. *Acta Geotechnica*, 13(1), 73-85.
- Song, X., and Khalili, N. (2019). A peridynamics model for strain localization analysis of geomaterials. *International Journal for Numerical and Analytical Methods in Geomechanics*, 43(1), 77-96.
- Song, X., and Menon, S. (2019). Modeling of chemo-hydromechanical behavior of unsaturated porous media: a nonlocal approach based on integral equations. *Acta Geotechnica*, 14(3), 727-747.

- Song, X., and Silling, S. (2020). On the peridynamic effective force state and multiphase constitutive correspondence principle. *Journal of the Mechanics and Physics of Solids*, 104-161.
- Sykora, D. W. Lower San Fernando Dam (California, 1971), ASDSO dam failures website, https://damfailures.org/case-study/lower-san-fernando-dam-california-1971/, posted September 2019.
- Trifunac, M. D., and Hudson, D. E. (1971). Analysis of the Pacoima dam accelerogram—San Fernando, California, earthquake of 1971. *Bulletin of the seismological Society of America*, 61(5), 1393-1411.
- Zienkiewicz, O. C., Chan, A. H. C., Pastor, M., Schrefler, B. A., and Shiomi, T. (1999). *Computational geomechanics* Chichester: Wiley.